Stress Field Simulation for Quantitative Ultrasound Elasticity Imaging

Lili Yuan and Peder C. Pedersen
Dept. of Electrical and Computer Engineering, Worcester Polytechnic Institute
Corresponding author: ECE department, 100 Institute Road, Worcester, MA, 01609, christinayuan@wpi.edu

Abstract: Finite element models using COMSOL Multiphysics 3.5a and 3.5a with MATLAB (COMSOL Inc., Burlington, MA) were developed to solve the problem of stress distribution interior homogeneous, isotropic, incompressible elastic solid material under known vertical external compression with a rectangular contact surface. Moreover, comparison between these results and analytical solutions was used to further validate that stress drops off with depth and laterally instead of being uniform which is assumed in most current elastography algorithms and thus results in artifacts darkening the image. Models with non-uniform external force and inhomogenous material property were also investigated for predictions of more complicated stress distribution.

Keywords: Elasticity imaging, Ultrasound transducer, stress distribution

1. Introduction

Elastography, combining the modern ultrasonic technology with the traditional concept of palpation for tumor, cancer and lesion detection, is an active area of research with already demonstrated clinical potential.

An important and challenging task in quantitative elasticity imaging development is the determination of the stress field due to force which is produced by the ultrasound transducer on the skin surface. Specifically, the need for accurate stress calculation results from the fact that the stiffness may be dependent on the magnitude and direction of the force exerted, especially if the linear stress-strain region (up to 1-2% strain) exceeds.

Finite Element Analysis (FEA), as a powerful computational tool to study the behavior of objects under external forces or deformations, has been applied to mechanical properties estimation and elasticity imaging development for human tissues by several research groups.

Based on FEA, Mutthieu Ferrant et al presented a physical-based deformable model for tracking physical deformation using image matching [1]. Yanning Zhu reported a novel Young's modulus reconstruction algorithm, in which only the force distribution at the compression surface is necessary, thus making the new method more practical [2]. A. P. C. Choi simultaneously obtained Young's modulus and Poisson's ratio of soft tissue by calculation of finite deformation effect produced by indentation [3]. Mark L. Palmeri simulated the dynamic response of tissues with spherical inclusions to an impulsive acoustic radiation force excitation from a linear array transducer [4]. Jessica R. Crouch et al introduced algorithms that generate a high quality hexahedral finite-element mesh and calculate boundary conditions automatically for prostate images registration [5]. Shengzheng Wang proposed an efficient approach for computing computed tomography (CT) numbers and calculated mechanical properties of bone tissue according to the relationship between tissue density and these CT numbers [6].

However, computation involved with FEA always is time consuming, even if for simple 3D model with coarse mesh in writer's experience, which may prevent the employment of FEA in real-time elastography.

Currently, we utilize FEA via COMSOL 3.5a to do forward stress distribution calculation inside isotropic material under known vertical external compression with a rectangular contact surface, purposing to further analyze simulation results from Love's equation [7] and obtain prediction for next step's experimental outcome on abdomen tissue-mimicking phantoms.

2. Methods

2.1 Experiment Set-Up

Experiments for external force measurement, stress calculation and elasticity imaging display were implemented on agar-based phantoms. Quasi-static force was applied through

transducer which was simultaneously connected to data acquisition and processing system, and measured by an array of force sensors mounted on the surface of the transducer.

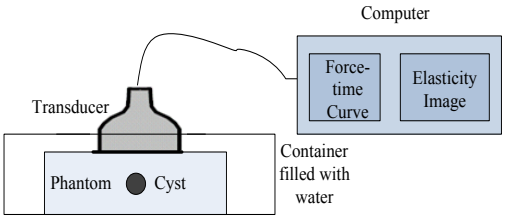

Figure 1. Experiment set-up for stress analysis and elasticity image display

2.2 Stress Field Calculation

The compressor is of length **2a** and width **2b** . The plane boundary (the closed curve obtained by connecting A, B, C, D in turn) of the semi-infinite solid is regarded as horizontal. The positive sense of the axis **z** is to be downwards in Cartesian co-ordinate system, and $\mathbf{x}, \mathbf{y}, \mathbf{z}$ to be coordinates of an arbitrary field point within the solid, and $\mathbf{x}', \mathbf{y}', \mathbf{0}$ to be one point on the plane boundary. The variables $\mathbf{a_1}$, $\mathbf{b_2}$, $\mathbf{c_3}$, $\mathbf{d_4}$ and **r** represent the distances to field point $(\mathbf{x}, \mathbf{y}, \mathbf{z})$ from point A, B, C, D and $(\mathbf{x}', \mathbf{y}', \mathbf{0})$, respectively.

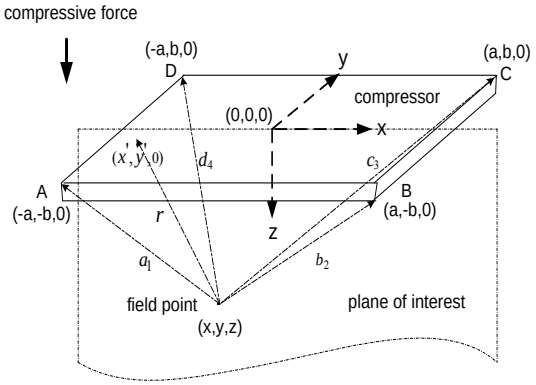

Figure 2. Compressor geometry with field point parameters in Cartesian co-ordinate system

Love's closed form solution [7] for the three dimensional (3D) stress component in a semi-infinite isotropic and incompressible solid due to a uniformly stressed rectangular compressor in **z** direction at a point (x, y, z) is

$$\sigma_{zz}(x,y,z) = \frac{1}{2\pi}\left[\frac{\partial V}{\partial z} - z\frac{\partial^2 V}{\partial z^2}\right]$$

where,

$$\frac{\partial V}{\partial z} = -p\{2\pi - \cos^{-1}\left[\frac{(a-x)(b-y)}{\sqrt{[(a-x)^2+z^2]\sqrt{[(b-y)^2+z^2]}}}\right] - \cos^{-1}\left[\frac{(a-x)(b+y)}{\sqrt{[(a-x)^2+z^2]\sqrt{[(b+y)^2+z^2]}}}\right] - \cos^{-1}\left[\frac{(a+x)(b-y)}{\sqrt{[(a+x)^2+z^2]\sqrt{[(b-y)^2+z^2]}}}\right] - \cos^{-1}\left[\frac{(a+x)(b+y)}{\sqrt{[(a+x)^2+z^2]\sqrt{[(b+y)^2+z^2]}}}\right]\},$$

$$\frac{\partial^2 V}{\partial z^2} = p\left\{\frac{a-x}{(a-x)^2+z^2}\left[\frac{b-y}{a_1}+\frac{b+y}{d_4}\right] + \frac{a+x}{(a+x)^2+z^2}\left[\frac{b-y}{b_2}+\frac{b+y}{c_3}\right] + \frac{b-y}{(b-y)^2+z^2}\left[\frac{a-x}{a_1}+\frac{a+x}{b_2}\right] + \frac{b+y}{(b+y)^2+z^2}\left[\frac{a-x}{d_4}+\frac{b+y}{c_3}\right]\right\}.$$

2.3 COMSOL Model Description

Stress distribution was computed using COMSOL module of 3D Structural Mechanics-Solid, Stress- Strain Analysis. Material geometry was 120 mm×120 mm×80 mm and compression area was 60 mm×20 mm. Since vertical external force was performed in a time interval shorter than stress relaxation, it can be regarded as static for one operation.

Table 1: Physical properties of agar-based tissue mimicking phantom

Young's modulus	5e4 Pa
Poisson's ratio	0.45
Density	1040 kg/m^3

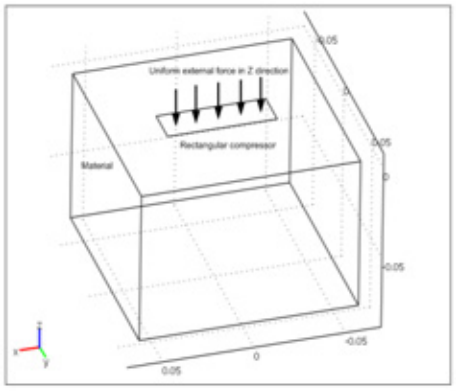

Figure 3. Model physical layout for isotropic, incompressible solid material under uniform external pressure

3. Simulation Results and Discussion

3.1 3D Stress Field

Figure 4 shows two charateristics of normal stress Szz distribution inside the material: stress magnitude decreases along depth and laterally; while stress concentrates at the periphery of compressor.

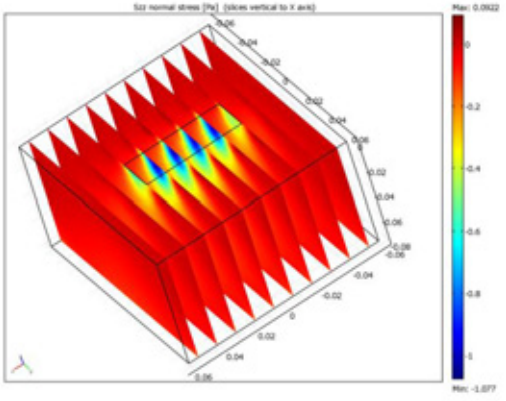

Figure 4. 3D cross-section slice for stress distribution along z direction

3.2 Comparison between Analytical Solution and FEA

Table 2: Parameters comparison between two methods

Method	Analytical method	FEA
Material		Young's modulus 5e4 Pa, Poisson's ratio 0.45, Density 1040 kg/m^3
Element Number	1185921	11607 Tetrahedral elements (computer memory limitation)
Solution time	16 second	124 second

Figure 5 displays stress decreasing with depth and laterally for both methods; on the other hand, there are discrepancies in different regions: firstly, stress singularity occurs around the top surface of solid material for FEA; secondly, at bottom of the material stress value from analytical method is smaller than FEA due to neglecting bottom reaction; finally, different lateral boundary estimations result in stress diversity at sides.

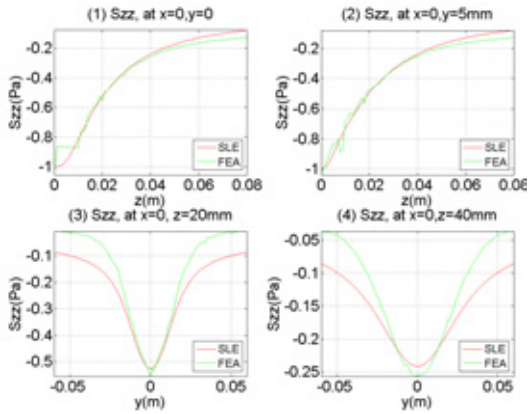

Figure 5. 1D stress distribution comparison between analytical method based on Love's Equation and FEA by COMSOL Multiphysics for the model in **Figure 1**. Normalized uniform external pressure along z axis, stress evaluated at the same field points

3.3 Stress Fields Prediction for Non-uniform External Pressure and Phantoms containing Tumors

As for Figure 6, part (1) shows stress drops off with decreasing external pressure along x axis and stress concentration happens at surface. The second part presents magnitude of normal stress changes dramatically around the periphery of tumor when tumor lies in pressure's influence region, attributed to the different mechanical properties between material and tumor.

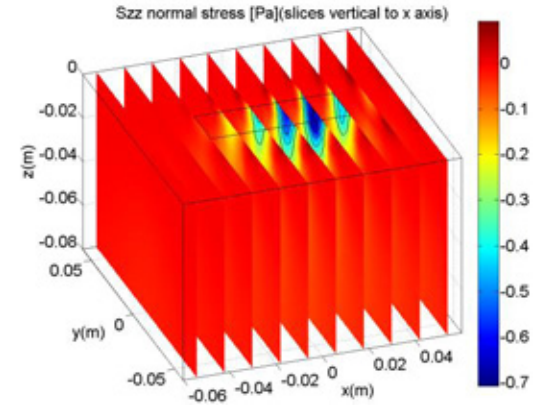

(1)

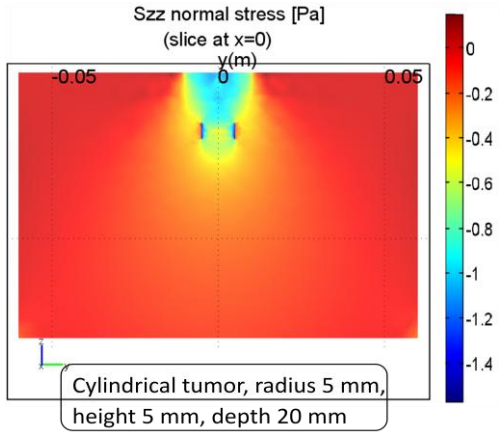

(2)

Figure 6. FEA simulation (1) non-uniform static loading P = 50/3*x-0.5 Pa; (2) with tumor inside the material, parameters for tumor: Young's modulus = 25e4 Pa, radius = 5 mm, height = 5 mm, depth = 10 mm, uniform external pressure along z axis

4. Conclusions and Future work

Agreement between analytical and finite element solutions shows stress dropping off with depth and laterally instead of being uniform which is assumed in most current elasticity imaging techniques and thus results in artifacts darkening the image.

Stress distribution for models with non-uniform external force and inhomogenous material property can be counterpart for ongoing experimental investigation on tissue mimicking phantoms.

Future work includes the modeling of phantoms with different degree of bonding tumors for more accurate boundary condition.

5. References

1. Mutthieu Ferrant , Simon K. Warfield, et al, 3D Image Matching Using Finite Element Based Elastic Deformation Model, *C. Taylor, A. Colchester (Eds.): MICCAI'99*, 202-210, (1999).

2. Yanning Zhu, Timothy J. Hall, and Jingfeng Jiang, A Finite-Element Approach for Young's Modulus Reconstruction, *IEEE Tran. on Med. Imag.* **22**, N0. 7, (2003).

3. A. P. C. Choi, Y. P. Zheng, Estimation of Young's modulus and Poisson's ratio of soft tissue from indentation using two different-sized indentors: finite element analysis of the finite deformation effect, *Med. Biol. Eng. Comput.*, **43**, 258-264, (2005).

4. Mark L. Palmeri, Amy C. Sharma, et al, A Finite-Element Method Model of Soft Tissue Response to Implusive Acoustic Radiation, *IEEE Tran. on Ultrasounics, Ferroelectrics, and Frequency Control*, **52**, No. 10, (2005).

5. Jessica R. Crouch, Stephen M. Pizer, et al, Automated Finite-Element Analysis for Deformable Registration of Prostate Images, *IEEE Tran. on Medical Imaging*, **26**, 1379-1390, (2007).

6. Shengzheng Wang, Jie Yang, Fast Mechanical Properties Estimation for Finite Element Model of Bone Tissue, *21st IEEE International Symposium on Computed-Based Medical Systems*, **18**, 147-149, (2008).

7. Love, A. E. H. The stress produced in a semi-infinite solid by pressure on part of the boundary. *Trans. of Royal Soc.*, **228**, London: Series A, (1929).